Understanding Precipitation Bias Sensitivities in E3SM-Multi-scale Modeling Framework from a Dilution Framework

Nana Liu[1], Michael S. Pritchard[1], Andrea M. Jenney[1], and Walter M. Hannah[2]

[1]Department of Earth System Science, University of California, Irvine, CA, USA
[2]Lawrence Livermore National Laboratory, Livermore, CA, USA

Key points:

1. Dimensionality of CRMs in the E3SM-MMF exhibits a striking effect on mean state precipitation patterns in subregions of the tropics.
2. MMFs tend to produce too many precipitating events but the use of 3D leads to fewer and is associated with signals of enhanced dilution.
3. Fast precursors of these climatological sensitivities are found that point to calibration targets for convection permitting global models.

Abstract

We investigate a set of Energy Exascale Earth System Model Multi-scale Modeling Framework (E3SM-MMF) simulations that vary the dimensionality and momentum transport configurations of the embedded cloud-resolving models (CRMs), including unusually ambitious 3D configurations. Issues endemic to all MMF simulations include too much ITCZ rainfall and too little over the Amazon. Systematic MMF improvements include more on-equatorial rainfall across the Warm Pool. Interesting sensitivities to CRM domain are found in the regional time-mean precipitation pattern over the tropics. The 2D E3SM-MMF produces an unrealistically rainy region over the northwestern tropical Pacific; this is reduced in computationally ambitious 3D configurations that use 1024 embedded CRM grid columns per host cell. Trajectory analysis indicates that these regional improvements are associated with desirably fewer tropical cyclones and less extreme precipitation rates. To understand why and how the representation of precipitation improved in 3D, we propose a framework that dilution is stronger in 3D. This viewpoint is supported by multiple indirect lines of evidence, including a delayed moisture-precipitation pickup, smaller precipitation efficiency, and amplified convective mass flux profiles and more high clouds. We also demonstrate that the effects of varying embedded CRM dimensionality and momentum transport on precipitation can be identified during the first few simulated days, providing an opportunity for rapid model tuning without high computational cost. Meanwhile the results imply that other less computationally intensive ways to enhance dilution within MMF CRMs may also be strategic tuning targets.

Plain Language Summary

The resolution of current climate models is not sufficient to resolve cloud and convective processes. Global cloud-resolving models (CRMs) have resolutions fine enough to represent individual cloud events but require too much computing power to be practical for large ensemble multi-decadal climate projection. Multi-scale modeling framework (MMFs) is an approach to simulate climate by embedding thousands of small CRMs interactively in each grid column of a planetary model. Trade-offs in how CRM is configured can affect the emergent behavior– we investigate this, including unusually ambitious 3D CRM configurations. Results show some interesting differences in the regional precipitation over the tropics. The 2D MMF produces an unrealistically rainy region over the northwestern tropical Pacific. Such biases are significantly reduced in 3D due to fewer tropical cyclones. To understand why and how the representation of precipitation improved in 3D, we propose a framework that mixing being stronger in 3D is a major part of the story. This is hard to prove directly but a few lines of circumstantial evidence support the case. Another upshot is that rapid effects of mixing that can be diagnosed in the first few days of global cloud resolving simulations should become tuning targets for optimizing longer-term statistics.

1. Introduction

Precipitation is a fundamental component of the Earth system, linked to clouds, moisture transport, and the global atmospheric circulation via latent heat release. Extreme precipitation events, for example hurricanes, floods, and droughts, can be life-threatening, and often lead to extensive socioeconomic losses. A number of studies have suggested that precipitation intensity will increase as the atmospheric moisture increases under a warming climate (Allen and Ingram, 2002; Donat et al., 2016; Norries et al., 2019; Sun et al., 2007; Trenberth et al., 2003;). Despite the socioeconomic importance of precipitation, the correct representation of precipitation is still a challenging task in climate models. Therefore, accurate knowledge of precipitation and how it can be realistically simulated is essential for understanding global and regional water and energy balances.

Global climate models (GCMs) capably simulate many features of the climatological spatial pattern of precipitation, although sometimes due to an incorrect combination of precipitation frequency and intensity (Dai et al. 1999; Sun et al. 2006). It has been reported that GCMs tend to produce an unrealistically high precipitation frequency but low intensity, even though precipitation amounts are realistic (Dai and Trenberth, 2004; DeMott et al., 2007; Zhou et al., 2008). Dai (2006) and Huang et al. (2017) also suggested that extreme precipitation is generally underestimated in most climate models. This is not surprising since precipitation is a result of processes that are mostly parameterized in current climate models, a difficult task due to their complexity. For example, cloud organization at mesoscales (Houze, 2004) can account for much of the Earth's precipitation and produce severe weather events and flooding. Lin et al. (2017) and Moncrieff et al. (2017) suggested that the conspicuous summer warm and dry bias over the central United States in one climate model is associated with the failure of that climate model in simulating mesoscale convective systems. However, no existing GCMs include a satisfactory parameterization of mesoscale cloud circulation. In other words, simulated precipitation in current models is still fairly incomplete and thus more understanding is required to correctly represent important mechanisms driving precipitation changes.

Cloud resolving models (CRMs) are attractive in this context as they have resolutions fine enough to represent individual cloud events, providing a wealth of information on cloud processes. While such models can be run globally for multiple months (Stevens et al. 2022) this is still impractical for the multi-decadal simulations required for most numerical climate science, pending additional increases in computing power or the capacity to better exploit it. Meanwhile, another promising approach to improve the representation of these small-scale processes is to use super-parameterization (SP), better known as the multi-scale modeling framework (MMF) approach to climate simulation, where the convective parameterization is replaced with a small, laterally periodic, and usually two dimensional (2D) CRM domain in each GCM grid column (Grabowski and Smolarkiewicz, 1999; Grabowski et al., 2001; Khairoutdinov et al., 2005; Khairoutdinov, 2016; Randall et al. 2003). While not without its own idealizations, MMF has shown significant improvement in simulating precipitation variability and statistics, such as the diurnal cycle of precipitation (Khairoutdinov et al., 2005; Pritchard and Somerville,2009), regional mesoscale convective system properties (Lin et al., 2021; Pritchard et al., 2011; Zhang et al., 2017), and rainfall intensity and extreme precipitation (Demott et al., 2007; Kooperman et al., 2016; Li et al., 2012). Furthermore, a number of studies have demonstrated the ability of MMF to improve intraseasonal-to-seasonal scale variability, such as the Madden-Julian

oscillation (Benedict and Randall, 2009), the South Asian Monsoon (Krishnamurthy et al., 2014), and the El Niño Southern Oscillation (Stan et al., 2010).

The MMF strategy discussed herein can be used with either 2D or 3D embedded CRMs in each GCM grid cell. In the classical 2D MMF, one issue is how to align the subgrid model within each large-scale model (i.e., east-west or north-south). Tulich (2015) suggested that tropical rainfall bias can be sensitive to the choice of CRM orientation. Khairoutdinov et al. (2005) suggested that the simulations based on the 2D MMF tend to produce an unrealistically humid and rainy region over the tropical western Pacific during the boreal summer, which was partially reduced through the use of the 3D MMF.

As the MMF approach exits its infancy and begins to be explored for potential operational use by major climate modeling centers (Hannah et al. 2020) it is important to understand the physical underpinnings of these chronic rainfall biases. Given their unique positioning to simulate climate with an approximation of convective processes that involves fewer assumptions relative to models with parameterized convection, a well-tuned MMF could be of interest for making climate predictions complementary to standard CMIP6 models.

But tuning MMF rainfall is an unfamiliar art especially regarding the novel knobs of CRM grid structure, dimensionality and formulation of momentum feedback. Currently, it is not clear why applying a 3D embedded model, which requires much more computational cost than a 2D embedded model and thus trades off against important throughput and cost constraints, can be useful to reduce the large precipitation bias over the tropical northwestern Pacific. Another under-explored issue is the effect of convective momentum transport (CMT), which on the one hand can impact the mean climate and the intraseasonal variability (Deng and Wu, 2010; Kim et al., 2008; Richter and Rasch, 2008; Wu and Yanai, 1994) but on the other hand is typically neglected in the implementation of most 2D versions of SP GCMs.

In this context, the goal of this study is to investigate the effects of varying embedded CRM dimensionality and momentum transport on the simulated precipitation in a state-of-the-art SP model. Practically, we hope to understand how to optimize the representation of tropical mean climate and its variability in MMFs. In the process, we seek new insight into the multi-scale physics that produce these emergent effects on the planetary water cycle, where the causality can become complicated when convection is made explicit.

The rest of this paper is organized as follows. Section 2 describes the simulations and observational data. Results in Section 3.1 we begin by comparing the climatology of seasonal precipitation climatology across MMF configurations and observations, followed by a trajectory analysis of precipitating events to understand variability behind the time mean, in section 3.2. Then, section 3.3 formulates a hypothetical explanation for a striking effect of dimensionality on the mean precipitation pattern. Section 3.4 and 3.5 present supporting evidence for the hypothesis. Finally, section 4 draws the conclusion and discusses the potential application and limitations of our results.

2. Data and Method

2.1 Model Simulations

The Energy Exascale Earth System Model MMF (E3SM-MMF) is a climate model, originally adapted from the SP Community Atmosphere Model (SP-CAM; Khairoutdinov et al., 2005), in which a CRM, here the System for Atmosphere Modeling (Khairoutdinov and Randall, 2003), is embedded within each grid cell of the E3SM atmosphere model (EAM; Rasch et al., 2019). In the conventionally parameterized EAM, turbulence, shallow cumulus cloud, and stratocumulus cloud are parametrized using the Cloud Layer Unified by Binormals (CLUBB) parametrization (Bogenshutz et al., 2013; Golaz et al., 2002). Deep convection is based upon the Zhang-McFarlane (ZM) scheme (Zhang and McFarlane, 1995) and cloud microphysics is parameterized using Morrison and Gettelman (MG2; Gettelman et al., 2015). Aerosol concentration and sea surface temperature are prescribed with present-day values. In the E3SM-MMF the convection and boundary layer turbulence parameterizations are replaced by embedded CRMs whose grid structure is not constrained by the grid spacing of the host GCMs. For 2D CRM configurations we use 32 CRM grid columns aligned in the north-south direction while the 3D has 32 x 32 grid columns with a grid spacing of 2 km. More details of the E3SM-MMF can be found in Hannah et al. (2020). All configurations of this study use a spectral element dynamical core on a cubed sphere geometry with 45 elements along each cube edge (ne45). Physics calculations, including the CRM of E3SM-MMF, are performed on a finite volume grid with 2x2 cells per element (ne45pg2). The physics grid is slightly coarser than the dynamics grid, but more closely matches the effective resolution of the dynamics grid (Hannah et al., 2021) and reduces the grid imprinting issue reported in Hannah et al. (2020). The simulations described here also utilize the CRM variance transport scheme of Hannah and Pressel (2022), which remedies an unphysical checkerboard pattern identified by Hannah et al. (2022).

Ten-year (2001-2010) E3SM-MMF 2D and 3D simulations are conducted for this study with climatological input data averaged over 1995-2005, such as solar forcing, aerosol concentration, and land surface types. For the 3D configuration this is a nontrivial computational expense that has only become approachable due to the advent of GPU supercomputing and recent efforts of the US Department of Energy (DOE) Exascale Computing Project to port the MMF's CRMs to run on GPU architectures.

To investigate the role of CMT, we conduct a pair of simulations with momentum coupling activated in 2D and 3D E3SM-MMF, respectively. Note that CMT in the 2D CRM is represented using the "explicit scalar momentum transport" (ESMT) scheme of Tulich (2015), while momentum feedback in the 3D CRM is directly handled by the MMF coupling scheme similar to other prognostic fields (Khairoutdinov et al., 2005). We also run another 10-year simulation with E3SMv2 (non-MMF) simulation for comparison. In summary, five simulations are used in this study hereafter non-MMF, 2D, 2D with CMT (2DM), 3D, and 3D with CMT (3DM).

2.2 Reanalysis and Observational Datasets

To assess the performance of E3SM-MMF's precipitation events, we use the fifth generation of reanalysis (ERA5) produced by the European Centre for Medium-Range Weather Forecasts (ECMWF; Hersbach et al., 2020) and the Global Precipitation Measurement Integrated Multi-satellitE Retrievals (IMERG). ERA5 provides hourly products near the surface and 37 pressure levels, with a horizontal resolution of 0.25°. Since reanalysis precipitation can be corrupted by the model-data fusion process intrinsic to data assimilation, we also include data from IMERG, which utilizes most of the GPM satellite constellation of passive microwave radiometers and

geostationary spaceborne infrared sensors in the passive microwave-sparse regions to produce half-hourly, 0.1° x 0.1° global precipitation products (Huffman et al., 2019). In order to compare directly with the model simulations, we regridded both the ten-year (2001-2010) ERA5 and IMERG data onto the same grid as E3SM output.

3. Results

3.1 Climatology of seasonal precipitation

Fig. 1 shows the mean global distribution of boreal summer (June-July-August, JJA) precipitation from observations and E3SM simulations. The solid and dashed lines in Fig. 1b-1f represent large positive and negative precipitation anomalies relative to observation (Fig. S1). To highlight the difference across MMF simulations, several strategic mean JJA precipitation difference maps are shown in Fig. 2.

In general, the E3SM-MMF models share some common local problems that are not seen in non-MMF simulations, such as too intense peak time-mean rainfall in the Pacific and Atlantic Intertropical Convergence Zone (ITCZ), and not enough over the northern Amazon (Fig. 1b-f). The boreal summer wet bias in the tropical Pacific and dry bias in Amazon are also reported by Kooperman et al. (2016) using the Community Earth System Model (CESM). However, the western Pacific bias is improved with SP-CAM in Kooperman et al. (2016), while it is only true in 3D E3SM-MMF (Fig. 1e and 1f). MMF increases equatorial rainfall over the Indian Ocean and western tropical Pacific, where it is too dry in non-MMF.

Interesting sensitivities to CRM dimensionality are found in specific subregions of the tropical Pacific (Fig. 2d, 2f) where a positive rainfall bias in excess of 2 mm/day occurs in both 2D MMF configurations (Fig. S1b, c) over the north western tropical Pacific (Fig. S2) and eastern tropical Pacific (0-20°N, 120-150°E). This problem has been noted in many published superparameterized simulations that use prescribed sea surface temperatures (e.g., DeMott et al., 2007; Kim et al., 2011; Khairoutdinov et al. 2005; Luo and Stephens, 2006), for reasons that remain poorly understood. Luo and Stephens (2006) suggested that the positive rainfall bias is related to an enhanced convective-wind-evaporation feedback because of the 2D geometry of CRM. However, Kim et al. (2011) demonstrated that similar precipitation bias appears in models with conventional parameterization. This wet bias over the northwestern tropical Pacific is largely removed with the use of a large, 3D CRM domain (Fig. S1d, e). Compared to the effects of CMT (Fig. 2c and 2e), the dimensionality has a much larger impact on the precipitation pattern (Fig. 2d and 2f).

3.2 Tropical cyclone tracking

As discussed above, dimensionality has a striking effect on the mean-state precipitation in JJA. The question naturally arises as to why, and whether a fundamental change in the characteristics of precipitating events, or their frequency, is responsible. It is well-known that tropical cyclones can account for a significant fraction of total precipitation. Therefore, it is possible that CRM dimensionality affects the characteristics of tropical cyclones. In this section, we use a Lagrangian feature-tracking approach to investigate the performance across MMF configurations, following events via their maximum relative vorticity at 850 hPa utilizing the TempestExtremes algorithm (Ullrich and Zarzycki, 2017; Ullrich et al. 2021). We use relative vorticity as an indicator of tropical cyclones because it focuses on smaller spatial scales than

pressure. To capture as many of the cyclones as possible, we perform event tracking over the entire tropics and the extra-tropics. Here we only consider storms lasting for more than a day (24 hours) to eliminate the detection of short-lived cyclones.

The overall pattern of cyclone trajectories in E3SM-MMF qualitatively resembles observations (Fig. S3), which reassures that the tracking algorithm is valid to use for model intercomparison. Track densities are shown in Fig. 3 for quantitative comparison. Note that due to a non-negligible Coriolis force required to maintain the cyclonic circulation, no storm tracks are near the equator where there exists large precipitation bias across E3SM-MMF simulations. Track density is calculated by counting the number of cyclones in each 1x1° grid point in the 3-hourly tracks for both model simulations and ERA5 reanalysis. The black contour lines represent the positive 2 mm/day precipitation anomaly compared to IMERG, which delineates the northwestern Pacific mean rainfall bias in the 2D MMF configurations (Fig. 2b, c). Consistent with the reduction of the tropical wet bias in this region, the population of tropical cyclones in 3DE3SM-MMF has dramatically decreased. Moreover, the dramatic decrease of tracked tropical cyclones over the western Pacific is coincident with reduced precipitation bias in 3D relative to 2D (Fig. S2d and 2f).

Fig. 4 shows the distribution of tracked cyclones aggregated spatially across 20°S-20°N. The number of tropical cyclones in all E3SM-MMF simulations is overestimated through all the lifetimes, compared to observations. However, this bias is reduced with both 3D and CMT, with dimensionality having a larger effect than the inclusion of CMT. This implies that a better understanding of the effect of dimensionality on precipitating event frequency may help reduce the precipitation bias in E3SM-MMF. The normalized histogram of storm durations (Fig. 4b) shows that all model configurations overestimate shorter-lived storms (duration < 8 days), and struggle to maintain longer-lived cyclones (duration > 9 days), but that neither momentum transport nor dimensionality dramatically affect these characteristics of tracked events. Similar conclusions can be drawn from extending the analysis to the 35°S-35°N band, with different magnitudes.

Fig. 5 shows the comparisons of other properties of tracked tropical cyclones, including relative vorticity at 850 hPa, precipitation rate, total column water, and relative humidity averaged over the area of 3 degrees of each track storm throughout all the lifetime. Precipitation that is associated with tropical cyclones is generally overestimated (Fig. 5a). The E3SM-MMF tends to produce too few weakly precipitating and too many strongly precipitating tropical cyclones, independent of its configuration. The magnitude of the precipitation bias for each precipitation rate is generally the same across all simulations. However, we note that rainfall from the heaviest precipitation events is reduced in 3D in comparison to 2D. A higher fraction of weaker vortex but a lower fraction of stronger vortex in all E3SM-MMF than in ERA5 is consistent with the finding that the E3SM-MMF struggles to maintain longer-lived tropical cyclones (Fig. 5b). Interestingly, the 3D simulations are characterized by higher total column water vapor and higher relative humidity than 2D, suggesting an important change in mean state. The relationship between column water vapor and precipitation will be further discussed in section 3.4.

In summary, so far our analysis of tracked vorticity events has shown that the interesting reduction in tropical northwest Pacific mean rainfall when 3D is used in place of 2D is driven, in part, by a strong reduction in the frequency of occurrence of precipitating events in this region.

3.3 Dilution hypothesis

The above analysis makes it clear that dimensionality has a striking effect on the mean state precipitation but has not resolved why. Signal in the column water vapor for tracked tropical cyclones offer a first clue. We suspect a dependence of the way cloudy and clear sky air mix with each other on CRM dimensionality. Petch et al. (2008) suggested that below 2 km, updrafts in 3D CRMs mix with the environment significantly more than updrafts in 2D CRMs, with updrafts in 3D CRMs both entraining and detraining larger fractions of their mass than in 2D. This matters given that dilution by entrainment of dry environmental air reduces updraft buoyancy, which can limit the development of convection in relatively dry columns. Petch et al. (2008) posed that a plume in three dimensions experiences larger fractional mixing than a plume of the same width in two dimensions because it has a greater surface area than a plume of the same width in two dimensions, and this leads to larger dilution by entrainment. This argument assumes that localized interfacial mixing and mass exchange is the same between 2D and 3D clouds, which may or may not be true. Additionally, a 3D updraft can diverge in more directions than a 2D updraft with the same mass flux, which would naturally cause more fractional detrainment and lead to more evaporation of cloud water and a lower precipitation efficiency. From this view, higher free-tropospheric humidity might be required to produce the same surface precipitation rate in a 3D CRM.

In the following section we will present evidence that suggests (although does not directly prove) that updrafts in the 3D MMF configurations exchange more mass with the environment than updrafts in 2D: A moisture-precipitation pickup that is shifted to higher background vapor, a smaller precipitation efficiency, and amplified convective mass flux profiles and high cloud fraction.

3.4 Evidence supporting a dimensionality-dilution framework

a. 3D shifts precipitation onset to a higher water vapor path

A well-known relationship between the column water vapor and precipitation has been identified by many studies (e.g., Bretherton et al., 2004; Muller et al., 2009; Peters and Neelin, 2006; Wolding et al., 2020), and dilution by entrainment processes has been revealed to be instrumental in explaining this relationship due to the differences in buoyancy between diluted and moist air (Kuo et al., 2017).

Fig. 6 shows the precipitation rate as a function of total vertically integrated precipitable water, or column water vapor (CWV) based on 3-hourly output from 10-year simulations. The critical CWV threshold (henceforth, “pickup”), at which there is a rapid increase of precipitation with CWV, occurs at different values in each simulation. The non-MMF exhibits a much earlier pickup than all the E3SM-MMF configurations.

The main point to take from Fig. 6 is that the precipitation pickup is shifted to higher background vapor in the E3SM-MMF simulations with 3D CRMs compared to 2D. This could be viewed as

consistent with our suspicion that there is weaker dilution by entrainment in 2D since convection that mixes less with its environment is less limited in its ability to produce precipitation by a drier free troposphere.

b. 3D reduces Precipitation efficiency

A corollary of the idea that more water vapor is required for the same amount of precipitation under a condition with more mixing is that precipitation efficiency is expected to be lower to overcome the stronger dilution barrier in 3D. Wilson and Toumi (2005) suggested that accumulated precipitation can be described as a triple product, in which precipitation can be expressed as proportional to three independent variables, including the mass flux, the specific humidity and the precipitation efficiency. Therefore, we define precipitation efficiency (PE) here as precipitation rate divided by the mass-weighted vertically integrated mass flux from CRM and specific humidity from 1000 to 5 hPa, which is derived from 10-year monthly outputs. Fig. 7 displays the box plot of PE values based on monthly output from ten-year E3SM-MMF simulations. Lines at each box represent (from bottom to top) the minimum, the 25th, 50th (median), 75th, and the maximum values. The open circles indicate the outliers. Consistent with our expectation, PE is lower in 3D, meaning that 2D precipitation is more than 3D for a given mass advection from the surrounding regions, in agreement with the stronger dilution hypothesis in 3D. Although dimensionality has a larger effect on this statistic than convective momentum transport, it is interesting to note the secondary sensitivity that E3SM-MMF with CMT in both 2D and 3D simulations have a higher PE than without momentum coupling.

c. 3D amplifies convective mass flux profiles and high cloud amounts.

Another line of evidence of increased entrainment and detrainment in 3D can be found in the statistics of the updraft mass flux by using 10-year monthly outputs (Fig. 8a). The updraft mass flux is obtained by multiplying the updraft speed greater than 2 m/s with air density when non-precipitating cloud water and ice content is greater than 1 g/kg. The larger low-level (around 700 hPa) peak in updraft mass flux in 3D indicates more sub-cloud entrainment than in 2D. Additionally, the difference between the low-level peak in updraft mass flux and the mid-tropospheric minimum around 400 hPa is larger in 3D than in 2D, indicating more detrainment in those simulations. This occurs despite a reduced boundary layer cloud liquid amount (Fig. 8c).

Jeevanjee and Zhou (2022) demonstrated that cloud resolving simulations with stronger mixing tend to also produce more high clouds, and this is also consistent with our simulations. Both 3D configurations of the MMF produce systematically higher cloud fraction and ice concentrations above 400 hPa (Figs. 8b, d). It is also interesting to note that something unusual occurred leading to extremely top-heavy convection and anomalously large high cloud fractions in just the 3D simulation that did not use convective momentum transport. It is interesting, but beyond the scope of this paper to investigate, that CMT modulated the high cloud amount so strongly in the 3D configuration, while having minimal impact in the 2D configuration.

Even though we cannot directly measure or assess dilution by entrainment in the current version of E3SM-MMF, multiple indirect lines of evidence have pointed to a change in it with dimensionality. As sketched in Fig. 9, 3D updrafts exchange more mass with the environment than 2D updrafts, leading to a stronger dilution by entrainment and more water vapor required

for convection to occur. Meanwhile, stronger dilution in 3D can result in more evaporation and a lower precipitation efficiency, leading to larger mass flux and more high clouds.

3.5 Fast-time scale effects during initialization & a connection to extremes.

We have provided quantitative support of the mechanism proposed in Fig. 9, namely that stronger dilution by entrainment in 3D leads to a higher rain pickup, a smaller PE, an increased updraft mass flux, and more anvil clouds. We now turn to a practical question as to whether these consequences of dimensionality could have been anticipated in just the first few days of sensitivity tests.

Fig. 10 shows comparison of the total grid-box liquid water path (boxplots summarize the geographic distribution of temporal snapshots) and the 99th percentile of vertical velocity at 500 hPa during the initialization of each simulation across MMF configurations. During the first day of the simulation, 2D produces more liquid water path than 3D (Fig. 10a), suggesting the fast response of dimensionality impact. We interpret the enhanced liquid in the 2D configuration as the signal of a system that is struggling less against mixing with its environment to maintain low level liquid water clouds. Moreover, the notable initial difference in the liquid path between 2D and 3D persists after one month (Fig. 10b). This implies that the long-term climatology of precipitating events can be predicted by these fast-time scale effects, providing an opportunity for rapid model tuning and optimization using short integrations without the high computational cost.

Fig. 10 also reveals an interesting response of extreme statistics to rainfall. Extreme grid point storms are more intense when a 2D CRM domain is used. Like the liquid cloud response, this geographic extreme signal is immediately detectable within the first simulated day, with the difference persisting over the subsequent month. Stronger extreme updrafts in 2D are consistent with the stronger tails of extreme precipitation that we noted in Fig. 5a. This is not immediately easy to reconcile as a consequence of entrainment and we do not attempt to explain the causal origins of the extreme response, other than to emphasize that two important aspects of a global cloud resolving simulation worth calibrating – time mean rainfall and extreme statistics – may both be controllable through the domain dimensionality of an MMF and might be possible to think about through a unified entrainment framework.

4. Concluding Discussion

In this study, we examined the representation of precipitation from a set of modern E3SM-MMF simulations that use different dimensionality and momentum transport, namely non-MMF, 2D, 2D with CMT, 3D, and 3D with CMT. Compared to previous MMF generations for whom computational limitations prohibited testing the effects of using ambitious 3D domains, the GPU-accelerated E3SM-MMF has penetrated new frontiers.

Compared to non-MMF, the E3SM-MMF produces too intense rainfall in ITCZ, and not enough rainfall over the northern Amazon. However, robust improvements due to MMF include increased on-equatorial rainfall over the Indian Ocean and western tropical Pacific, where it is too dry in non-MMF. Most interestingly, the results reveal some distinct differences in the mean-state precipitation pattern over subregions of the tropics across the multiple MMF configurations. For instance, the 2D MMF produces an unrealistically rainy region over the

northwestern and eastern tropical Pacific, while these regional biases are significantly reduced when a large, 3D CRM is used in E3SM-MMF. In comparison to the striking effect of dimensionality, impacts of convective momentum transport (CMT) are minor in reducing this precipitation bias. Trajectory analysis indicates that these regional improvements of time-mean precipitation simulation in the northwestern and eastern tropical Pacific are associated with fewer tropical cyclones in 3D E3SM-MMF, rather than a fundamental change in their character.

In attempting to understand why and how the representation of precipitation is improved in 3D E3SM-MMF, we have proposed a framework – that dilution by entrainment is stronger in 3D relative to 2D. Conceptually, this is rooted in two simple geometric ideas: an updraft in 3D has more surface area to mix with the environment than an updraft of the same width in 2D, and a 3D updraft can diverge in more directions than a 2D updraft with the same mass flux. Empirically, it can be connected to multiple sensitivities we observed across our experiments. Stronger dilution of dry air reduces updraft buoyancy and suppresses convection until the lower troposphere is sufficiently moistened, meaning more water vapor is required for rain pickup; delayed rainfall pickup is seen in our 3D MMF configurations (Fig. 6). An associated reduced precipitation efficiency requires a larger convective mass flux, resulting in more high clouds (Fig. 9). Consistent with fewer barriers to low cloud liquid content from environmental mixing, the 2D MMF also initially generates and then sustains more cloud liquid water during the initialization. The 3D simulations also have reduced extreme rainfall rates and grid point storm magnitudes.

We demonstrate that precursor signals suggestive of the significant difference in the mean state precipitation and extreme tail behavior across E3SM-MMF configurations can be identified even in the first few simulated days of output. This may provide an opportunity for rapid model tuning to improve precipitation representation in the climate model and advance the understanding of mechanisms driving precipitation events.

The findings of this study raise a number of questions and potential future research topics. Wet-ITCZ and dry-Amazon biases appear to be a recurring bias in the current generation of E3SM-MMF; it will be interesting to discover whether ocean coupling impacts these signals, or whether tuning strategies can address them. An obvious limitation of our analysis is that no direct observations of entrainment or dilution exist for quantitative confirmation. Rather, the proposed dilution framework is supported by mechanisms that are associated with the dilution by entrainment as displayed in the summary diagram (Fig. 9). Nevertheless, our results are generally consistent with other studies (Jeevanjee and Zhou, 2022; Petch et al., 2008; Phillips and Donner, 2006; Tompkins and Semie, 2017). For example, Tompkins and Semie (2017) explored the role of entrainment in convection organization. They argued that the strength of updraft dilution by entrainment controls the onset of convective organization. With cloud-resolving simulations, Jeevanjee and Zhou (2022) indicate that an increase in cloud fraction with horizontal resolution can be traced back to enhanced horizontal mixing, which increases evaporation of condensed water and decreases precipitation efficiency, consequently resulting in an increased mass flux and more high cloud. The consistency of our results with previous studies using different models imply that the findings of this study are not model dependent.

Another considerable caveat of this work is that the impact of CMT remains unclear, and we have not focused on it, despite some interesting evidence of impact especially in 3D. Several results of this study suggest that the influence of CMT on the mean-state precipitation and extreme precipitation is not as significant as the dimensionality. However, momentum coupling is implicated in some intriguingly strong sensitivities of the 3D E3SM-MMF. Without CMT, 3D MMF tends to exhibit a much later rain pick-up, a large increase in high cloud amount and associated convective mass flux, and lower values of PE. This highlights the importance of CMT in the more accurate representation of precipitating events in climate models. We note that the 3D E3SM-MMF that includes CMT compared best against rainfall observations in our initial analysis.

Finally, the notable difference between 2D and 3D during the initiation implies that the first week or month of simulation can be treated as a forecast for longer-term behavior. Initial signals like low cloud liquid content and extreme storm development may be helpful precursors for tuning longer term regional rainfall anomalies, and could be viewed as consistent through a dilution framework. If confirmed, this could provide an additional constraint in quick model validation and comparison across different configurations. The 3D MMF configurations explored in this study were not trivial to compute, but made possible by GPU supercomputing through the Exascale Computing Project. With global storm resolving simulations remaining expensive yet increasing in popularity, precursor signals that can be linked to climatological calibration targets of mean rainfall and extreme skill are of high interest today.

Finally, a preliminary investigation of convection size during the first month of model initiation suggested that convection can develop into more organized convection in 3D. As shown in Fig. S4, precipitation events tend to be larger in 3D than in 2D, with the mean volumetric rain (a product of precipitation area and the mean rain rate) smaller. Given the importance of precipitation to global and regional water and energy balances, further exploration of how dimensionality and momentum affect convection organization seems warranted.

Acknowledgements

This research was supported by the Exascale Computing Project (17-SC-20-SC), a collaborative effort of the U.S. Department of Energy Office of Science and the National Nuclear Security Administration. This work was performed under the auspices of the U.S. Department of Energy by Lawrence Livermore National Laboratory under Contract DE-AC52-07NA27344. The analysis of this study is performed using computational resources provided by the National Energy Research Scientific Computing Center (NERSC), a DOE Office of Science User Facility supported by the Office of Science of the U.S. The ERA5 data can be obtained from https://www.ecmwf.int/en/forecasts/datasets/reanalysis-datasets/era5. The IMERG precipitation products can be downloaded from Goddard Earth Sciences Data and Information Services Center (GES DISC) (https://disc.gsfc.nasa.gov/).

References:

Ahmed, F., and Schumacher, C. (2015), Convective and stratiform components of the precipitation-moisture relationship, *Geophys. Res. Lett.*, **42**, 10,453– 10,462, doi:10.1002/2015GL066957.

Allen, M. R., & Ingram, W. J. (2002). Constraints on future changes in climate and the hydrological cycle. *Nature*, **419**, 224–232.

Benedict, J. J., and D. A. Randall (2009), Structure of the Madden-Julian oscillation in the superparameterized CAM, *J. Atmos. Sci.*, **66**(11), 3277–3296.

Bretherton, C. S., Peters, M. E., & Back, L. E. (2004). Relationships between Water Vapor Path and Precipitation over the Tropical Oceans, *Journal of Climate*, ***17*(7)**, 1517-1528. https://journals.ametsoc.org/view/journals/clim/17/7/1520-0442_2004_017_1517_rbwvpa_2.0.co_2.xml

Cohen, C. (2000). A Quantitative Investigation of Entrainment and Detrainment in Numerically Simulated Cumulonimbus Clouds, *Journal of the Atmospheric Sciences*, ***57*(10)**, 1657-1674. https://journals.ametsoc.org/view/journals/atsc/57/10/1520-0469_2000_057_1657_aqioea_2.0.co_2.xml

Dai, A., (2006), Precipitation characteristics in eighteen coupled climate models. *J. Climate*, **19**, 4605–4630, https://doi.org/10.1175/JCLI3884.1.

DeMott, C. A., Klingaman, N. P., Tseng, W.-L., Burt, M. A., Gao, Y., & Randall, D.A. (2019) The convection connection: How ocean feedbacks affect tropical mean moisture and MJO propagation. *Journal of Geophysical Research Atmospheres*, **124**, 11910– 11931. https://doi.org/10.1029/2019JD031015

DeMott, C. A., Randall, D. A., & Khairoutdinov, M. (2007). Convective precipitation variability as a tool for general circulation model analysis. *Journal of Climate*, **20**, 91–112. https://doi-org.manowar.tamucc.edu/10.1175/JCLI3991.1

Deng, L., and X. Wu, (2010), Effects of convective processes on GCM simulations of the Madden–Julian oscillation. *J. Climate*, **23**, 352–377.

Donat, M. G., Lowry, A. L., Alexander, L. V., O'Gorman, P. A., & Maher, N. (2016). More extreme precipitation in the world's dry and wet regions. *Nature Climate Change*, **6**, 508–513.

Gettelman, A., & Morrison, H. (2015). Advanced two-moment bulk microphysics for global models. Part I: Off-line tests and comparison with other schemes. *Journal of Climate*, **28**(3), 1268–1287. https://doi.org/10.1175/JCLI-D-14-00102.1

Grabowski, W. W., 2001: Coupling cloud processes with the large-scale dynamics using the Cloud-Resolving Convection Parameterization (CRCP). *J. Atmos. Sci.*, **58,** 978–997

Grabowski, W. (2016), Towards global large eddy simulation: Super-parameterization revisited, *J. Meteorol. Soc. Jpn.*, **94**, 327–344.

Grabowski, W. W., and P. K. Smolarkiewicz, 1999: CRCP: A Cloud Resolving Convection Parameterization for modeling the tropical convecting atmosphere. *Physica D*, **133 ,** 171–178.

Hannah, W. M., Jones, C. R., Hillman, B. R., Norman, M. R., Bader, D. C., Taylor, M. A., et al. (2020). Initial results from the super-parameterized E3SM. *Journal of Advances in Modeling Earth Systems*, **12**(1), e2019MS001863. https://doi.org/10.1029/2019MS001863

Hannah, W. M., Bradley, A. M., Guba, O., Tang, Q., Golaz, J.-C., and Wolfe, J.: Separating Physics and Dynamics Grids for Improved Com- putational Efficiency in Spectral

Element Earth System Models, Journal of Advances in Modeling Earth Systems, 13, e2020MS002 419, https://doi.org/10.1029/2020MS002419, 2021.
Hannah, W., Pressel, K., Ovchinnikov, M., and Elsaesser, G.: Checkerboard patterns in E3SMv2 and E3SM-MMFv2, Geosci. Model Dev., 15, 6243–6257, https://doi.org/10.5194/gmd-15-6243-2022, 2022.
Hannah, W. and Pressel, K.: Transporting CRM Variance in a Multiscale Modelling Framework, EGUsphere [preprint], https://doi.org/10.5194/egusphere-2022-397, 2022.
Hersbach, H., and Coauthors, 2020: The ERA5 global reanalysis. *Quart. J. Roy. Meteor. Soc.*, **146**, 1999–2049, https://doi.org/10.1002/qj.3803.
Hohenegger, C., & Stevens, B. (2013). Preconditioning Deep Convection with Cumulus Congestus, *Journal of the Atmospheric Sciences*, ***70*(2)**, 448-464. https://journals.ametsoc.org/view/journals/atsc/70/2/jas-d-12-089.1.xml
Houze, R. A. (2004), Mesoscale convective systems, *Rev. Geophys.*, 42, RG4003, doi:10.1029/2004RG000150.
Houze, R. A., Jr., Chen, S. S., Kingsmill, D. E., Serra, Y., & Yuter, S. E. (2000). Convection over the Pacific Warm Pool in relation to the Atmospheric Kelvin-Rossby Wave, *Journal of the Atmospheric Sciences*, ***57*(18)**, 3058-3089. https://journals.ametsoc.org/view/journals/atsc/57/18/1520-0469_2000_057_3058_cotpwp_2.0.co_2.xml
Huang, D.-Q., P. Yan, J. Zhu, Y. Zhang, X. Kuang, and J. Cheng, (2017). Uncertainty of global summer precipitation in the CMIP5 models: A comparison between high-resolution and low-resolution models. *Theor. Appl. Climatol.*, **132**, 55–69, https://doi.org/10.1007/s00704-017-2078-9.
Huffman, G. J., Stocker, E. F., Bolvin, D. T., Nelkin, E. J., & Tan, J. (2019). *GPM IMERG final precipitation L3 half hourly 0.1 degree x 0.1 degree V06*. Retrieved from Greenbelt, MD: Goddard Earth Sciences Data and Information Services Center (GES DISC). https://doi.org/10.5067/GPM/IMERG/3B-HH/06.
Jeevanjee, N., & Zhou, L. (2022). On the resolution-dependence of anvil cloud fraction and precipitation efficiency in radiative-convective equilibrium. *Journal of Advances in Modeling Earth Systems*, **14**, e2021MS002759. https://doi.org/10.1029/2021MS002759
Khairoutdinov, M. F., & Randall, D. A. (2003). Cloud resolving modeling of the ARM summer 1997 IOP: Model formulation, results, uncertainties, and sensitivities. *Journal of the Atmospheric Sciences*, **60**(4), 6072–625. https://doi.org/10.1175/1520-0469(2003)060<0607:crmota>2.0.co;2
Khairoutdinov, M., Randall, D., & DeMott, C. (2005). Simulations of the Atmospheric General Circulation Using a Cloud-Resolving Model as a Superparameterization of Physical Processes, *Journal of the Atmospheric Sciences*, ***62*(7),** 2136-2154. https://journals.ametsoc.org/view/journals/atsc/62/7/jas3453.1.xml
Klingaman, N. P., & Demott, C. A. (2020). Mean-state biases and interannual variability affect perceived sensitivities of the Madden–Julian oscillation to air–sea coupling. *Journal of Advances in Modeling Earth Systems*, **12**, e2019MS001799. https://doi.org/10.1029/2019MS001799
Kim, D., J.-S. Kug, I.-S. Kang, F.-F. Jin, and A. T. Wittenberg, (2008), Tropical Pacific impacts of convective momentum transport in the SNU coupled GCM. *Climate Dyn.*, **31**, 213–226.

Kooperman, G., M. Pritchard, M. Burt, M. Branson, and D. Randall (2016), Robust effects of cloud superparameterization on simulated daily rainfall intensity statistics across multiple versions of the Community Earth System Model, *J. Adv. Model. Earth Syst.*, **8**, 140–165, doi:10.1002/2015MS000574.

Krishnamurthy, V., Stan, C., Randall, D. A., Shukla, R. P., & Kinter, J. L., III. (2014). Simulation of the South Asian Monsoon in a Coupled Model with an Embedded Cloud-Resolving Model, *Journal of Climate*, ***27*(3)**, 1121-1142. https://journals.ametsoc.org/view/journals/clim/27/3/jcli-d-13-00257.1.xml

Kuo, Y., Neelin, J. D., & Mechoso, C. R. (2017). Tropical Convective Transition Statistics and Causality in the Water Vapor–Precipitation Relation, *Journal of the Atmospheric Sciences*, ***74*(3)**, 915-931. https://journals.ametsoc.org/view/journals/atsc/74/3/jas-d-16-0182.1.xml

Li, F., Rosa, D., Collins, W. D., and Wehner, M. F. (2012), "Super-parameterization": A better way to simulate regional extreme precipitation?, *J. Adv. Model. Earth Syst.*, **4**, M04002, doi:10.1029/2011MS000106.

Lin, Y., W. Dong, M. Zhang, Y. Xie, W. Xue, J. Huang, and Y. Luo, (2017), Causes of model dry and warm bias over central U.S. and impact on climate projections. *Nat. Commun.*, **8**, 881, https://doi.org/10.1038/s41467-017-01040-2.

Mapes, B. E., & Neale, R. B. (2011). Parameterizing convective organization to escape the entrainment dilemma. *Journal of Advances in Modeling Earth Systems*, **3**, M06004.

Moncrieff, M. W., Liu, C., & Bogenschutz, P. (2017). Simulation, Modeling, and Dynamically Based Parameterization of Organized Tropical Convection for Global Climate Models, *Journal of the Atmospheric Sciences*, ***74*(5),** 1363-1380. Retrieved Jul 7, 2022, from https://journals.ametsoc.org/view/journals/atsc/74/5/jas-d-16-0166.1.xml

Muller, C. J., Back, L. E., O'Gorman, P. A., and Emanuel, K. A. (2009), A model for the relationship between tropical precipitation and column water vapor, *Geophys. Res. Lett.*, **36**, L16804, doi:10.1029/2009GL039667.

Neelin, J. D., Peters, O., & Hales, K. (2009). The Transition to Strong Convection, *Journal of the Atmospheric Sciences*, ***66*(8),** 2367-2384. https://journals.ametsoc.org/view/journals/atsc/66/8/2009jas2962.1.x

Norris, J., Chen, G., & Neelin, J. D. (2019). Thermodynamic versus dynamic controls on extreme precipitation in a warming climate from the community Earth system model large ensemble. *Journal of Climate*, **32**, 1025–1045.

Petch, J.C., Blossey, P.N. and Bretherton, C... (2008), Differences in the lower troposphere in two- and three-dimensional cloud-resolving model simulations of deep convection. Q.J.R. Meteorol. Soc., **134:** 1941-1946. https://doi.org/10.1002/qj.315

Peters, O., and J. D. Neelin (2006), Critical phenomena in atmospheric precipitation. *Nature Physics*, **2**, 393–396, doi:10.1038/nphys314.

Phillips, V.T.J. and Donner, L.J. (2006), Cloud microphysics, radiation and vertical velocities in two- and three-dimensional simulations of deep convection. Q.J.R. Meteorol. Soc., **132**: 3011-3033. https://doi.org/10.1256/qj.05.171

Pritchard, M. S., M. W. Moncrieff, and R. C. J. Somerville (2011), Orogenic propagating precipitation systems over the United States in a global climate model with embedded explicit convection, *J. Atmos. Sci.*, **68**(8), 1821–1840.

Randall, D., Khairoutdinov, M., Arakawa, A., & Grabowski, W. (2003). Breaking the Cloud Parameterization Deadlock, *Bulletin of the American Meteorological Society*, ***84*(11)**, 1547-1564. https://journals.ametsoc.org/view/journals/bams/84/11/bams-84-11-1547.xml

Rasch, P. J., Xie, S., Ma, P.-L., Lin, W., Wang, H., Tang, Q., et al. (2019). An overview of the atmospheric component of the energy exascale Earth system model. *Journal of Advances in Modeling Earth Systems*, **11**(8), 2377–2411. https://doi.org/10.1029/2019MS001629

Redelsperger, J.-L., Brown, P.R.A., Guichard, F., How, C., Kawasima, M., Lang, S., Montmerle, T., Nakamura, K., Saito, K., Seman, C., Tao, W.K. and Donner, L.J. (2000), A gcss model intercomparison for a tropical squall line observed during toga-coare. I: Cloud-resolving models. Q.J.R. Meteorol. Soc., **126:** 823-863. https://doi.org/10.1002/qj.49712656404

Richter, J. H., and P. J. Rasch, (2008), Effects of convective momentum transport on the atmospheric circulation in the Community Atmosphere Model, version 3. *J. Climate*, **21**, 1487–1499.

Sohn, B. J., Ryu, G., Song, H., & Ou, M. (2013). Characteristic Features of Warm-Type Rain Producing Heavy Rainfall over the Korean Peninsula Inferred from TRMM Measurements, *Monthly Weather Review*, ***141*(11)**, 3873-3888. https://journals.ametsoc.org/view/journals/mwre/141/11/mwr-d-13-00075.1.xml

Stevens, B., Satoh, M., Auger, L., Biercamp, J., Bretherton, C. S., Chen, X., & Düben, P. (2019). DYAMOND: the DYnamics of the Atmospheric general circulation Modeled On Non-hydrostatic Domains. *Progress in Earth and Planetary Science*, ***6*(1).** https://link.gale.com/apps/doc/A601368192/AONE?u=mlin_oweb&sid=googleScholar&xid=ac0339e3

Sun, Y., S. Solomon, A. Dai, and R. W. Portmann (2007), How often will it rain? *J. Clim.*, **20**, 4801–4818, doi:10.1175/JCLI4263.1.

Tompkins, A. M., and Semie, A. G. (2017), Organization of tropical convection in low vertical wind shears: Role of updraft entrainment, *J. Adv. Model. Earth Syst.*, **9**, 1046– 1068, doi:10.1002/2016MS000802.

Trenberth, K. E., A. Dai, R. M. Rasmussen, and D. B. Parsons (2003), The changing character of precipitation, *Bull. Am. Meteorol. Soc.*, **84**, 1205–1217, doi:10.1175/BAMS-84-9-1205.

Tulich, S. N. (2015), A strategy for representing the effects of convective momentum transport in multiscale models: Evaluation using a new superparameterized version of the Weather Research and Forecast model (SP-WRF), *J. Adv. Model. Earth Syst.*, **7**, 938– 962, doi:10.1002/2014MS000417.

Ullrich, P. A., & Zarzycki, C. M. (2017). Tempestextremes v1.0: A framework for scale-insensitive pointwise feature tracking on unstructured grids. *Geoscientific Model Development*, **10**, 1069– 1090.

Ullrich, P. A., Zarzycki, C. M., McClenny, E. E., Pinheiro, M. C., Stansfield, A. M., & Reed, K. A. (2021). TempestExtremes v2.1: a community framework for feature detection, tracking, and analysis in large datasets. *Geoscientific Model Development*, ***14*(8)**, 5023. https://link.gale.com/apps/doc/A671970002/AONE?u=mlin_oweb&sid=googleScholar&xid=d4de7f8d

Wilson, P. S., and Toumi, R. (2005), A fundamental probability distribution for heavy rainfall, *Geophys. Res. Lett.*, **32**, L14812, doi:10.1029/2005GL022465.

Wolding, B. O., J. Dias, G. Kiladis, F. Ahmed, S. W. Powell, E. Maloney, and M. Branson, 2020: Interactions between moisture and tropical convection. Part I: The

coevolution of moisture and convection. *J. Atmos. Sci.*, **77**, 1783–1799, https://doi.org/10.1175/JAS-D-19-0225.1.

Wolding, B., Dias, J., Kiladis, G., Maloney, E., & Branson, M. (2020). Interactions between Moisture and Tropical Convection. Part II: The Convective Coupling of Equatorial Waves, *Journal of the Atmospheric Sciences*, *77***(5)**, 1801-1819. https://journals.ametsoc.org/view/journals/atsc/77/5/jas-d-19-0226.1.xml

Wu, X., and M. Yanai, (1994), Effects of vertical wind shear on the cumulus transport of momentum: Observations and parameterization. *J. Atmos. Sci.*, **51**, 1640–1660.

Zhang, G. J., & McFarlane, N. A. (1995). Sensitivity of climate simulations to the parameterization of cumulus convection in the Canadian Climate Centre general circulation model. *Atmosphere-Ocean*, **33**(3), 407–446. https://doi.org/10.1080/07055900.1995.9649539.

Zhang, K., Fu, R., Shaikh, M. J., Ghan, S., Wang, M., Leung, L. R., … Marengo, J. (2017). Influence of superparameterization and a higher-order turbulence closure on rainfall bias over Amazonia in Community Atmosphere Model version 5. *Journal of Geophysical Research: Atmospheres*, **122**. 9879– 9902, https://doi.org/10.1002/2017JD026576

Zhou, T. J., Yu, R. C., Chen, H. M., Dai, A., & Pan, Y. (2008). Summer precipitation frequency, intensity, and diurnal cycle over China: A comparison of satellite data with rain gauge observations. *Journal of Climate*, **21**, 3997–4010.

716 Figures

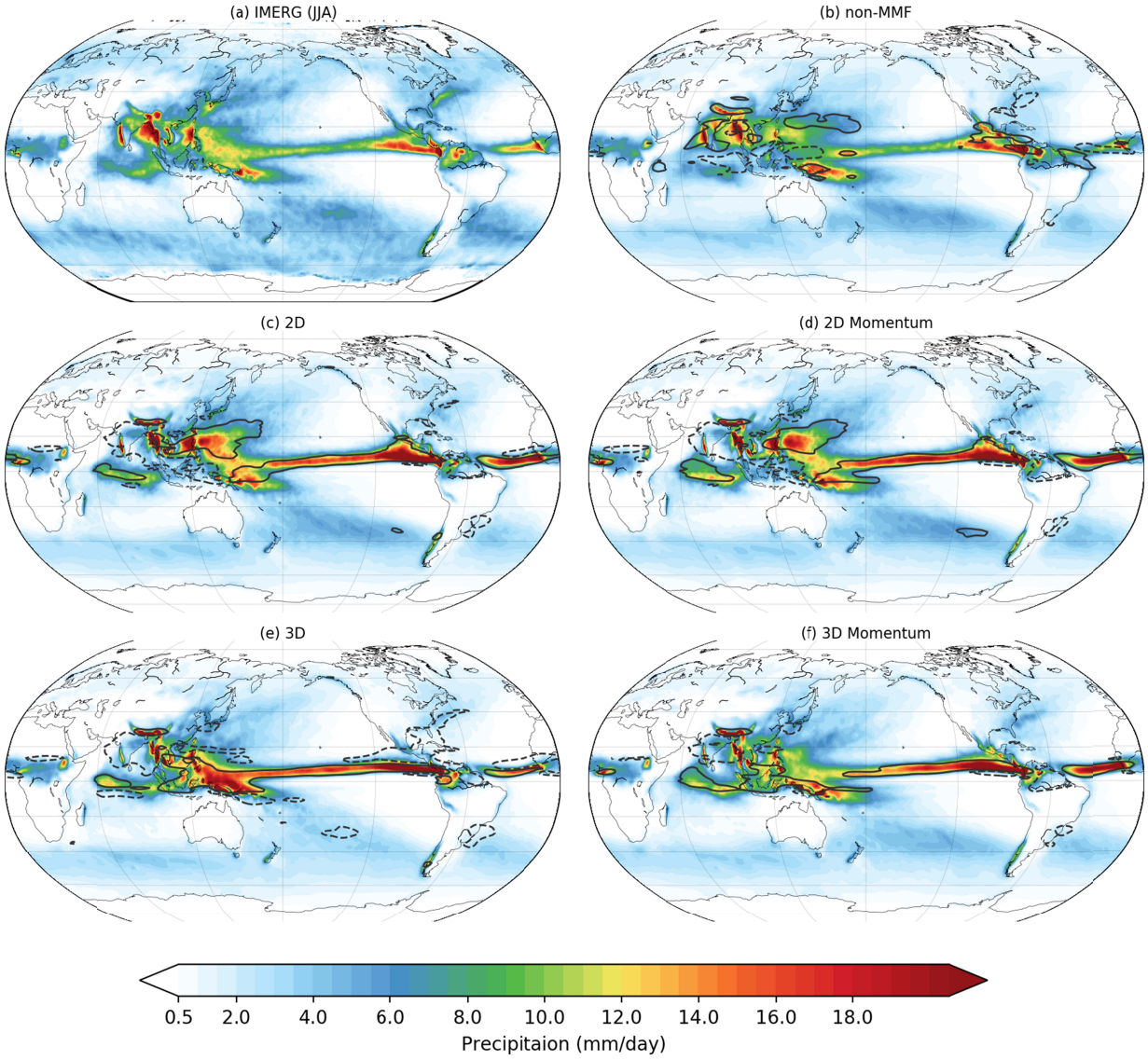

717
718 Fig. 1 Climatological distribution of total precipitation in June-July-August (JJA), (a) IMERG,
719 (b) non-MMF, (c) 2D, (d) 2DM, (e) 3D, (f) 3DM. The solid (dashed) lines in (b)-(f) indicate +(-)
720 2 mm/day precipitation anomaly as shown in Figure S1.

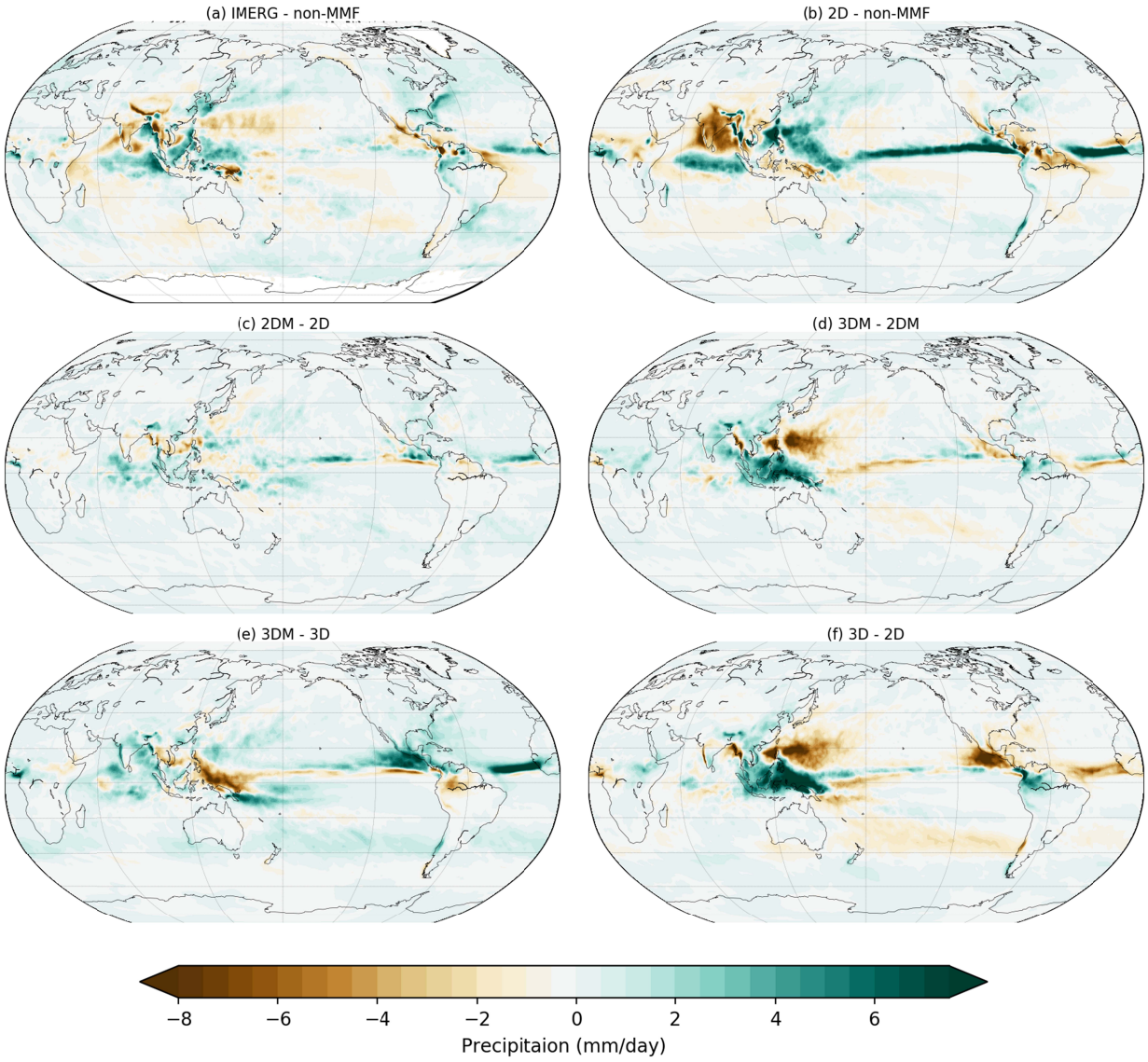

Fig. 2 Mean JJA precipitation difference between (a) IMERG and non-MMF, (b) 2D and non-MMF, (c) 2DM and 2D, (d) 3DM and 3D, (e) 3DM and 3D, (f) 3D and 2D.

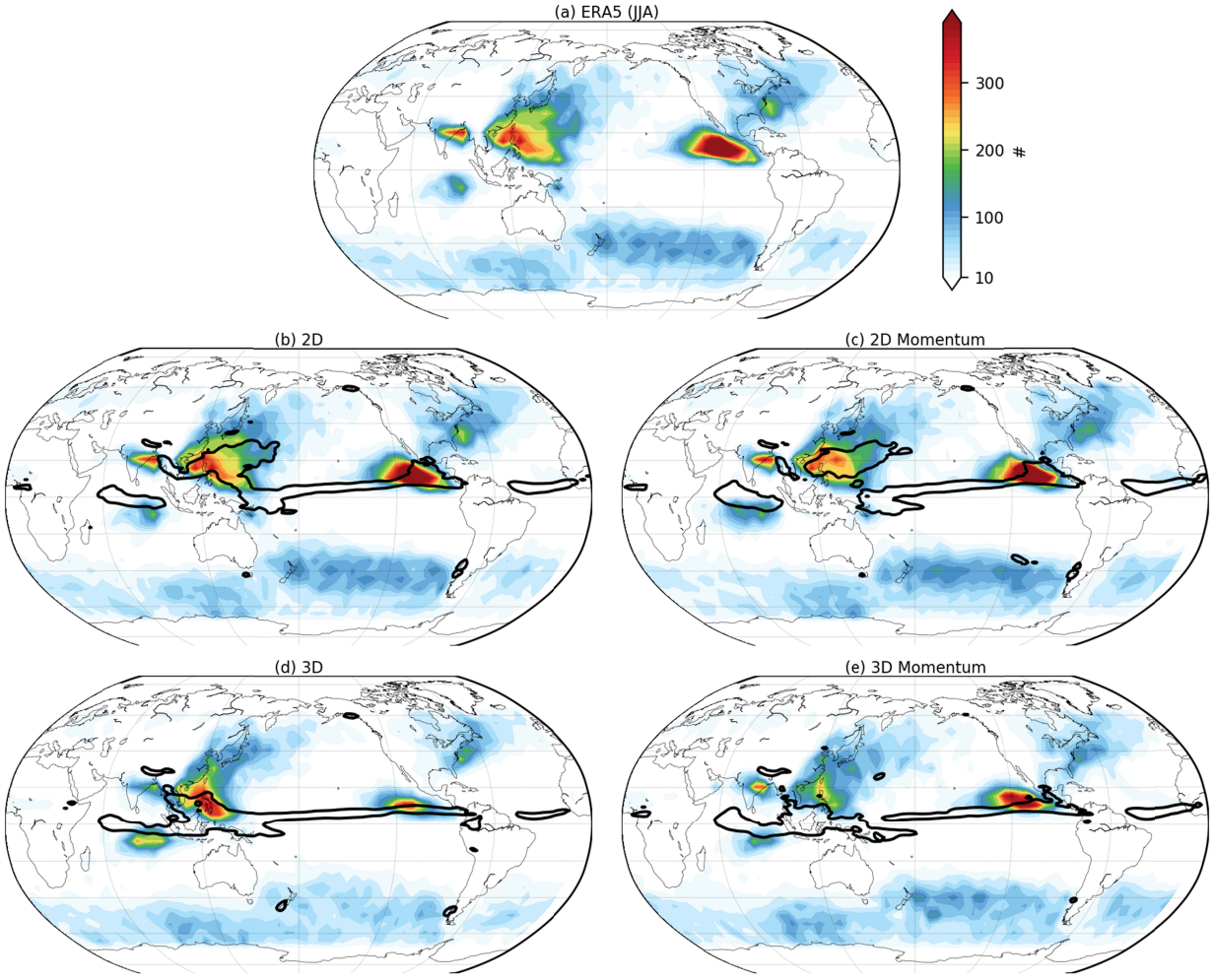

Fig. 3 Cyclone track density from (a) ERA5, (b) 2D, (c) 2DM, (e) 3D, (f) 3DM. Black lines in panels (b)-(f) represent positive 2 mm/day precipitation anomaly compared to IMERG.

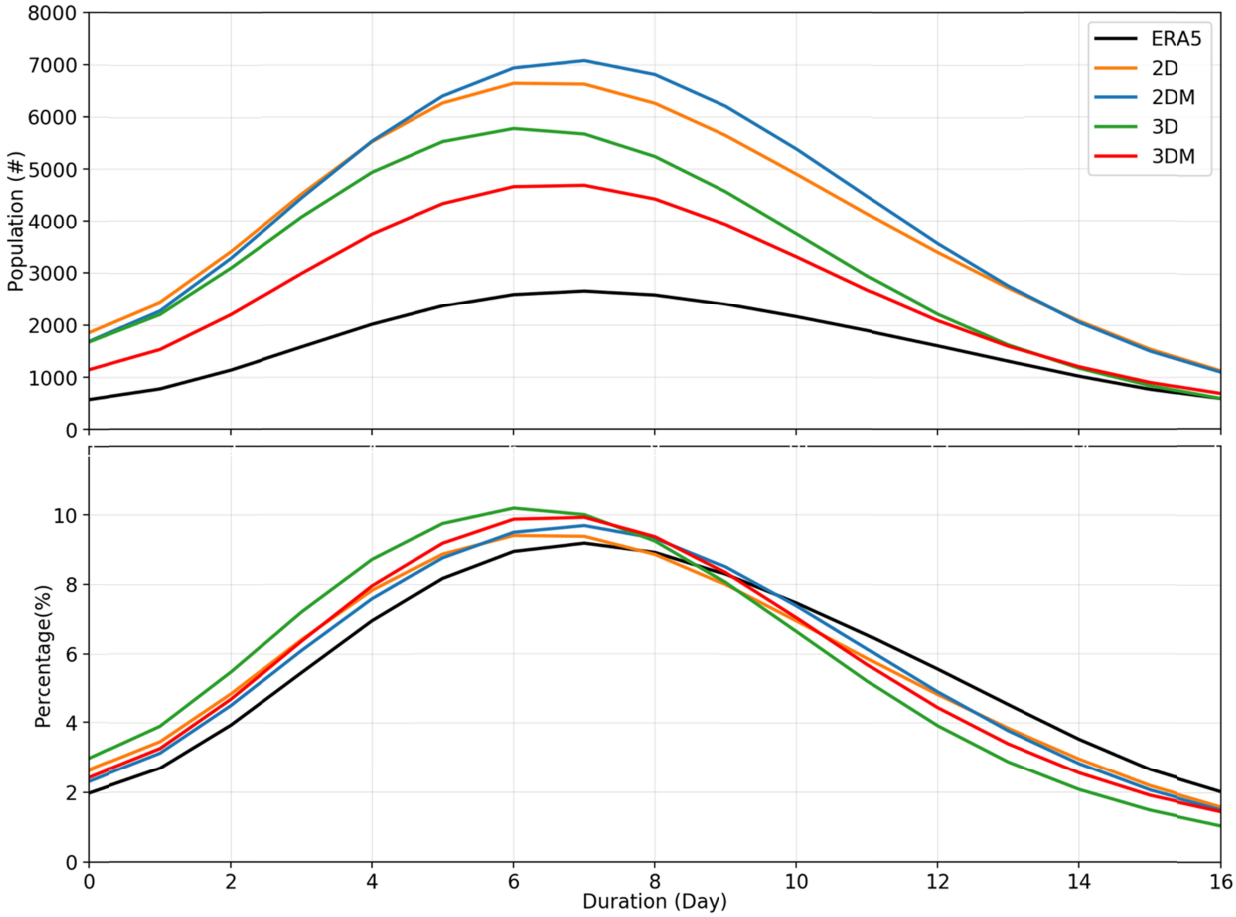

Fig. 4 Histogram of total (a) and normalized (b) tropical cyclone durations (20°S-20°N) from ERA5 and E3SM-MMF simulations.

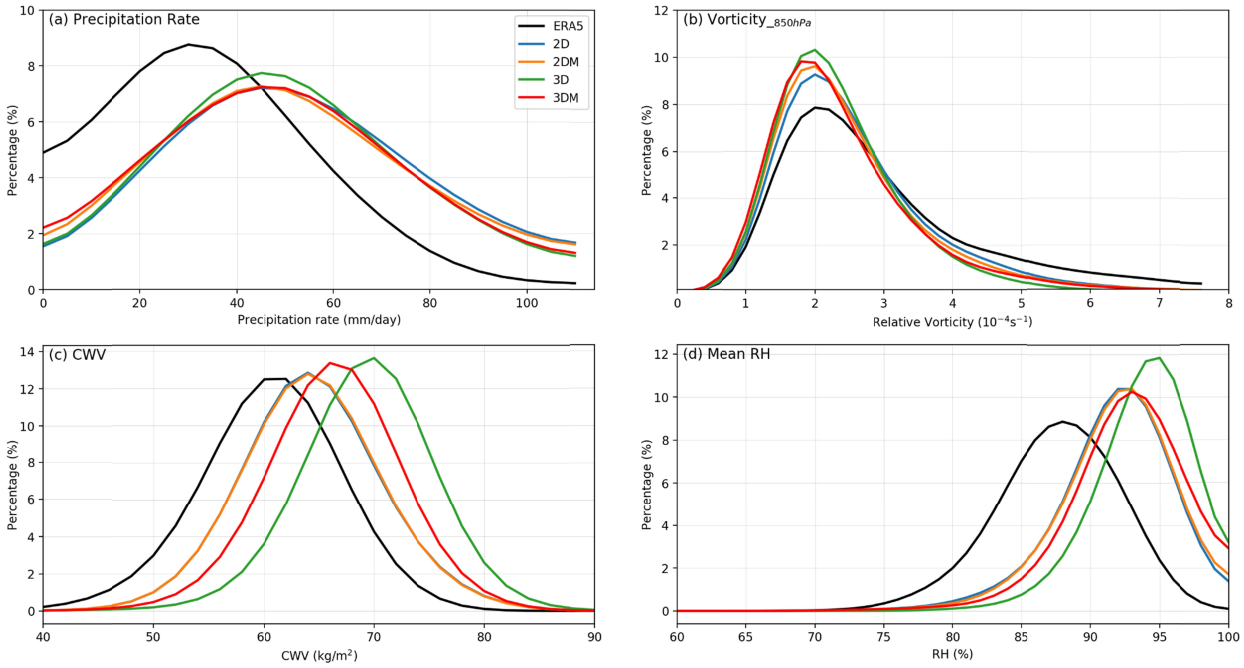

Fig. 5 Properties of tracked tropical cyclones, (a) precipitation rate, (b) relative vorticity at 850 hPa, (c) column water vapor, (d) column-averaged relative humidity.

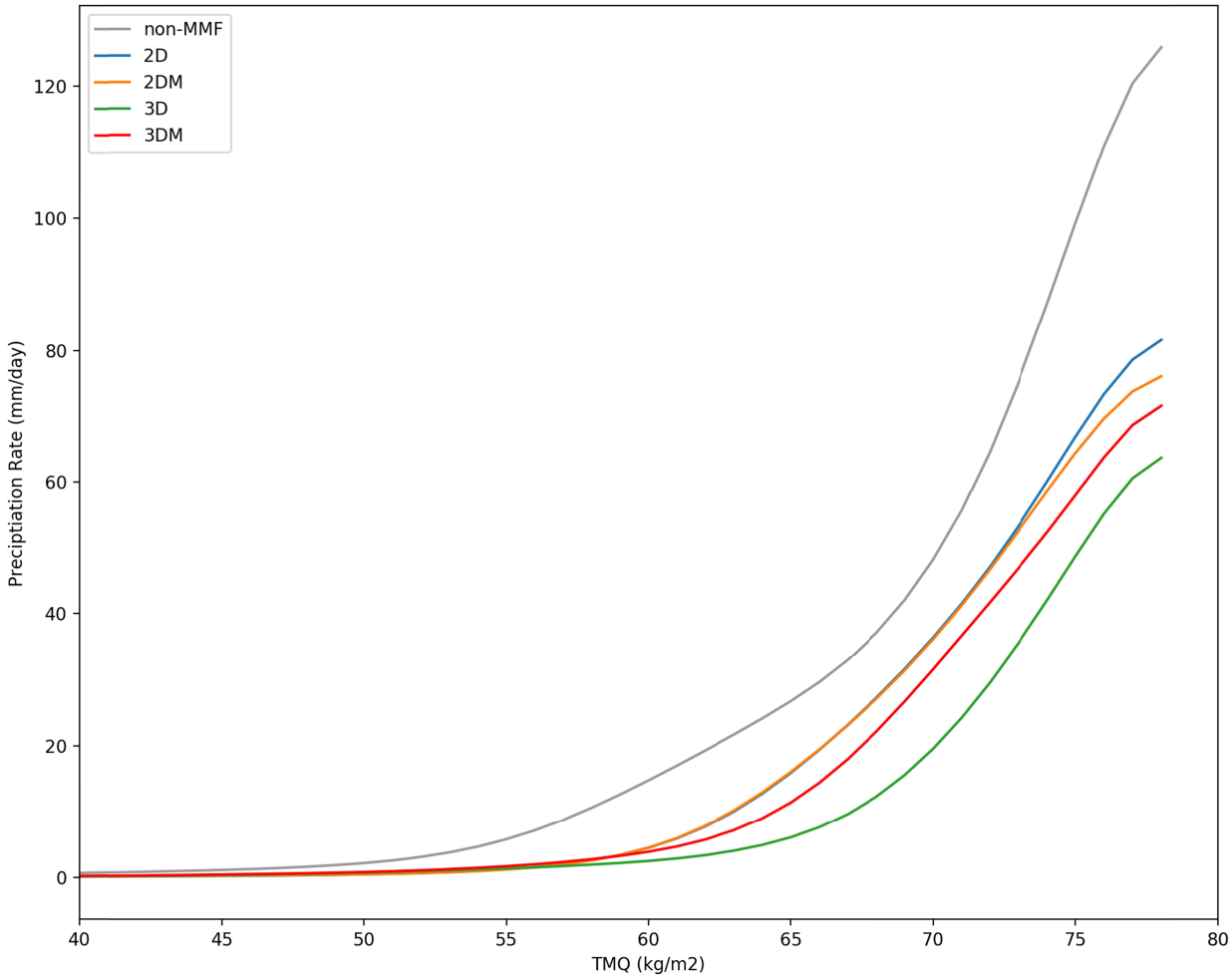

Fig. 6 Relationship between precipitation rate and total precipitation water over tropical western Pacific.

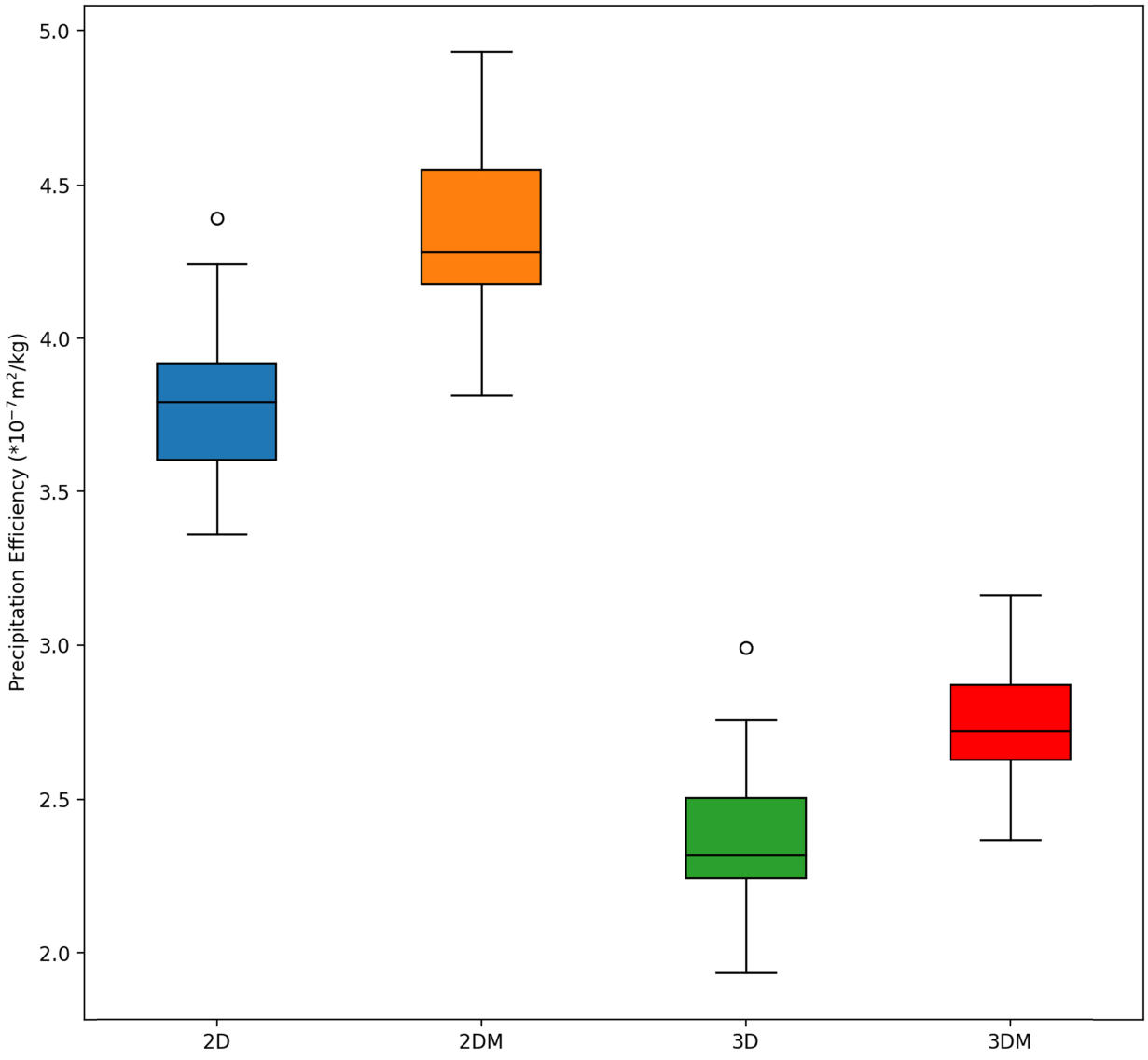

Fig. 7 Boxplot of precipitation efficiency across E3SM-MMF configurations. Lines at each box represent (from bottom to top) the minimum, the 25th, 50th (median), 75th, and the maximum values.

744
745

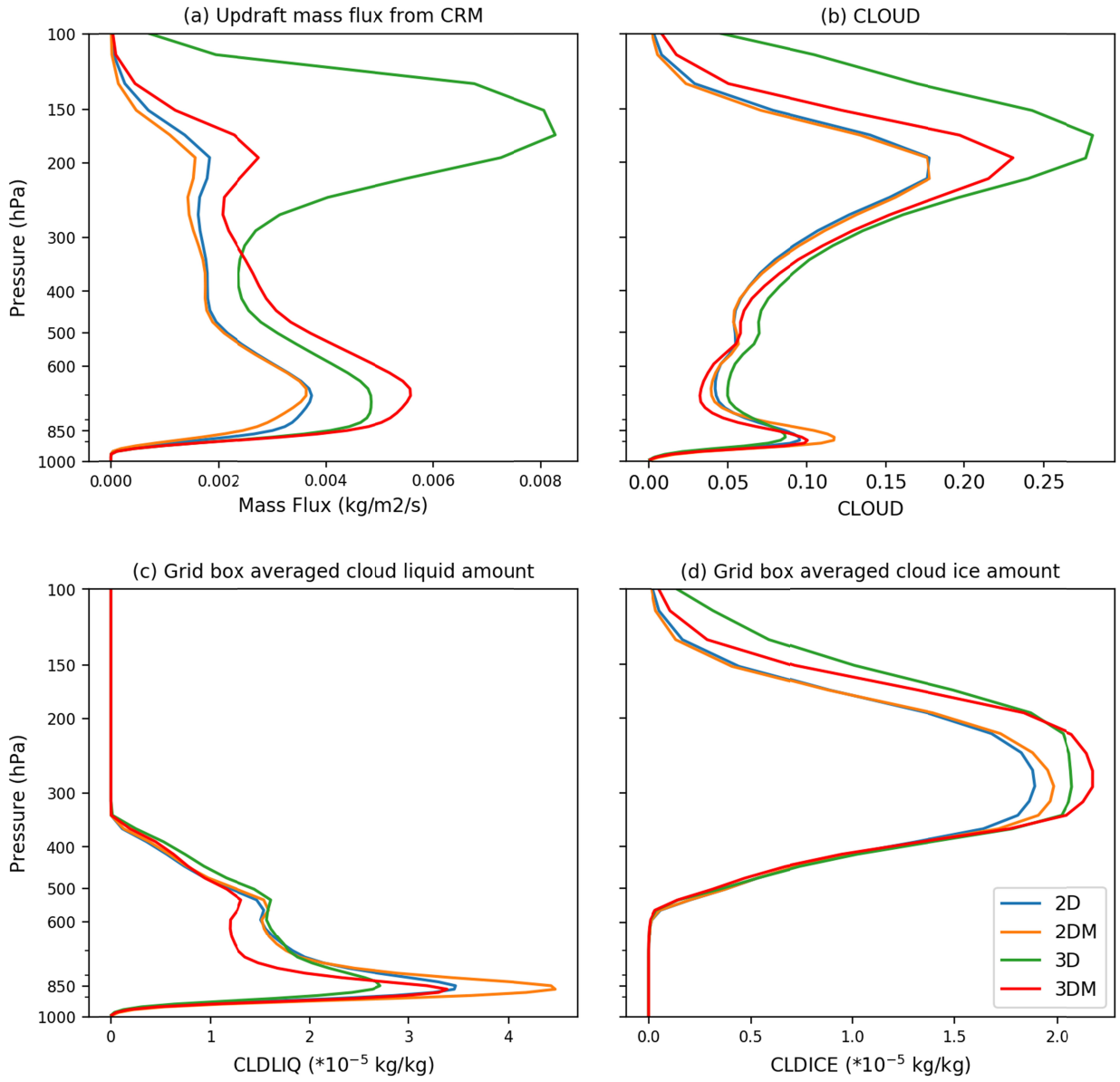

746
747

748 Fig. 8 Profiles of (a) updraft mass flux, (b) cloud fraction, (c) cloud liquid amount, (d) cloud ice
749 amount across E3SM-MMF configurations. The profiles are derived from tropics (20°S-20°N).

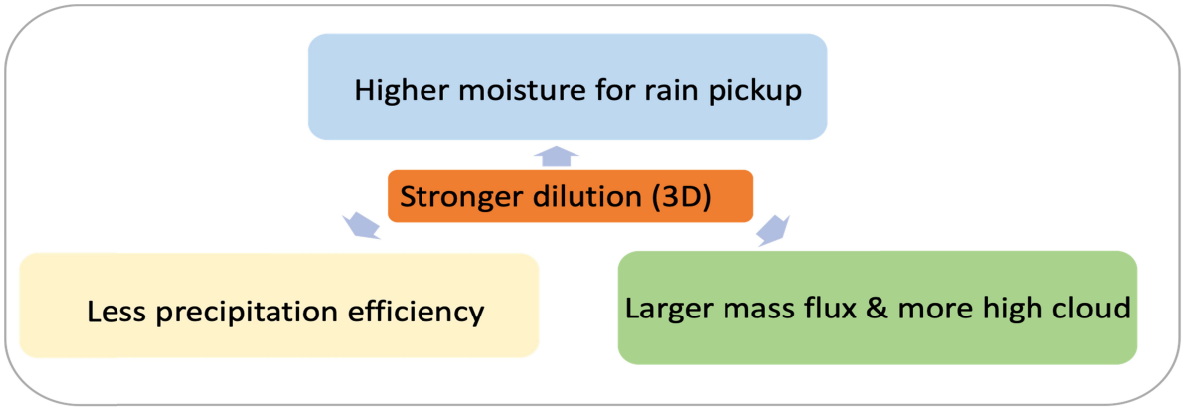

750
751 Fig. 9 Diagram of a dilute framework with multiple indirect lines of supportive evidence.
752

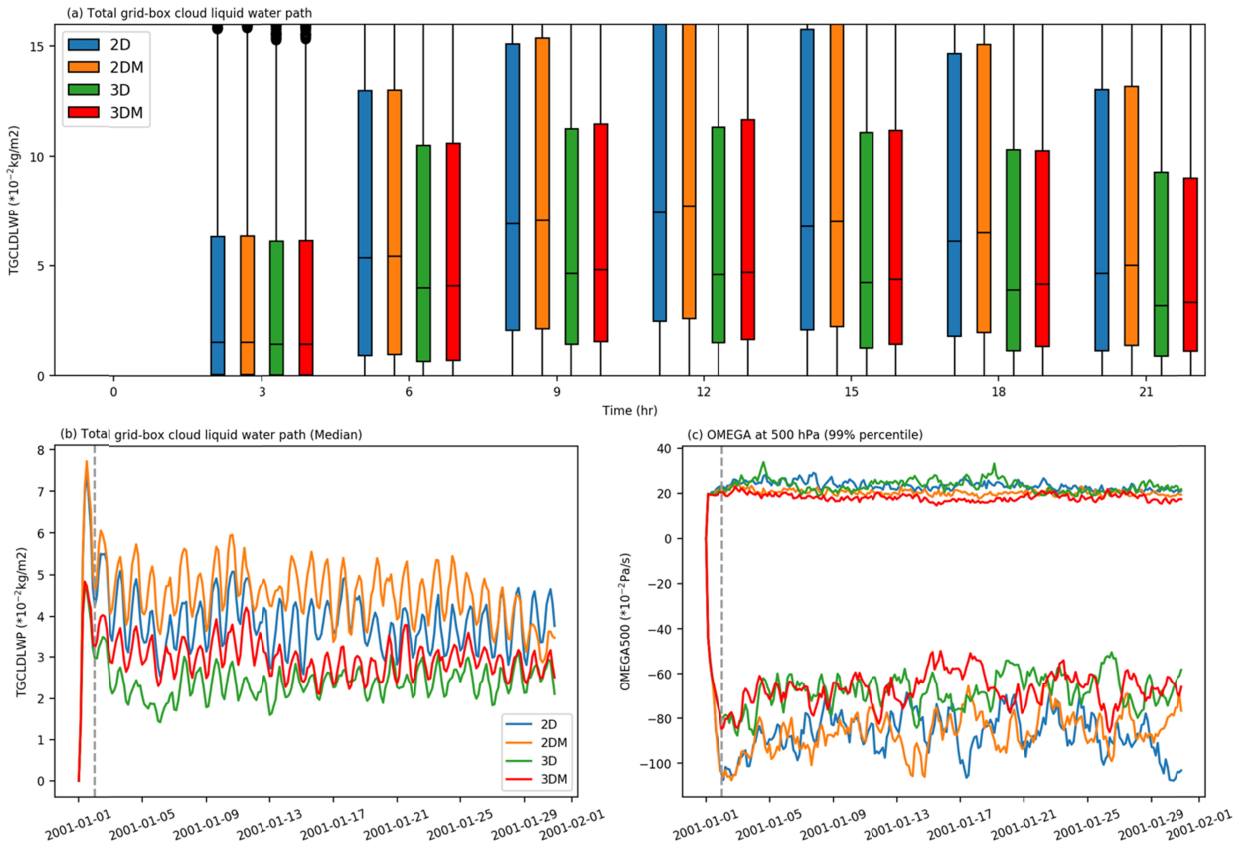

Fig. 10 Comparison of liquid water path and omega at 500 hPa during initialization across E3SM-MMF configurations: (a) boxplot of total cloud liquid water path during the first day of initialization, (b) median of total cloud liquid water path for the first month of simulations, (c) 99% percentile omega at 500 hPa.